PROCEEDINGS, 48th Workshop on Geothermal Reservoir Engineering
Stanford University, Stanford, California, February 6-8, 2023
SGP-TR-224

Multidisciplinary collaboration to create a new numerical model of the Lahendong geothermal field

John O'Sullivan[1]*, Fathan Abdurachman[3], Greg Bignall[4], Chris Bromley, Ken Dekkers[1], Muhammad Ghassan[2], Michael Gravatt[1], Pudyo Hastuti[3], Astri Indra[2], Rony Nugraha[12], Fernando Pasaribu[3], Joris Popineau[1], Imam Prasetyo[3], Vicky Rai[2], Theo Renaud[1], Jeremy Riffault[1], Dhanie Yuniar[3], Michael O'Sullivan[1]

[1]Department of Engineering Science, University of Auckland, Private Bag 92019, Auckland, New Zealand

[2]Geoenergi Solusi Indonesia (Geoenergis), Cibis Nine 11th Floor, Jakarta, Indonesia

[3]PT. Pertamina Geothermal Energy, Jakarta, 10340, Indonesia

[4]G&A Geothermal Advice Limited, Taupo 3330, New Zealand

*jp.osullivan@auckland.ac.nz

Keywords: Lahendong, Geothermal reservoir simulation, Integrated modelling, AUTOUGH2, Waiwera

ABSTRACT

Indonesia has the second highest geothermal power installed capacity worldwide and expects to develop more geothermal energy in the future. In the north-east of the Sulawesi Island, the high temperature geothermal system of Lahendong has a current installed capacity of 80 MWe. It lies in the Minahasa-Sangihe Volcanic Arc resulting from the subduction beneath the Celebes Sea Plate. The wells drilled reveal temperatures in the range of 200-320°C and a high degree of control from the existence of a caldera, an active regional fault network and intense hydrothermal alteration.

In this paper we discuss a multidisciplinary approach to a new modelling study of the Lahendong Geothermal Field (LGF). The project team included members from PT. Pertamina Geothermal Energy, the Geothermal Institute at the University of Auckland, Geoenergis Solusi Indonesia, and independent New Zealand geothermal experts. It successfully achieved its objectives through close collaboration and an inclusive, transparent approach.

A review and update of the conceptual model of the LGF has been conducted. The updated conceptual model was set up as a digital conceptual model in the Leapfrog software and used to develop a new numerical model. In setting up the numerical model we use an integrated modelling framework developed at the University of Auckland that allows the direct creation of a numerical model from a Leapfrog-based digital conceptual model. The numerical model can be run in AUTOUGH2, a local variant of the industry-standard simulator TOUGH2, or in Waiwera, a highly parallelised, open-source simulator developed by the University of Auckland and GNS Science.

The new numerical model was calibrated against the measured data using the industry-standard approach. The state of model calibration achieved is good and therefore, we are confident that the model provides a good representation of the LGF and is appropriate to use for forecasting.

1. INTRODUCTION

Lahendong is a high-enthalpy liquid dominated geothermal field located 30 km south of Manado on the northern arm of the island of Sulawesi, Indonesia (Figure 1). The first well drilled at Lahendong in 1983 reached a temperature of 260°C at a depth of 660 m and discharged acidic fluids (Surachman et al., 1987). Since then, there have been 39 wells drilled for exploration, production, reinjection and monitoring, measuring temperatures up to 350°C. The first 20 MWe power plant were commissioned in 2000 (Hochstein and Sudarman, 2008). As of 2022, the Lahendong Geothermal Field (LGF) has an installed capacity of 80 MWe from four units.

More recent wells, drilled between 2016 and 2019 have provided important new information about the geothermal system. In 2022 a collaborative project to study the LGF was initiated between PT. Pertamina Geothermal Energy (PGE), the Geothermal Institute at the University of Auckland (UoA), Geoenergis Solusi Indonesia (Geoenergis) and independent New Zealand geothermal experts. The objective of the project was to carry out a detailed resource assessment of the system using the most up-to-date data, analyses, and numerical modelling techniques. There were several stages involved in the project:

1. Reviewing the updated field data
2. Updating the conceptual model
3. Updating the Leapfrog digital conceptual model
4. Reviewing the existing numerical model
5. Developing a new numerical modal
6. Calibrating the numerical model
7. Using model forecast to assess the future potential of the LGF

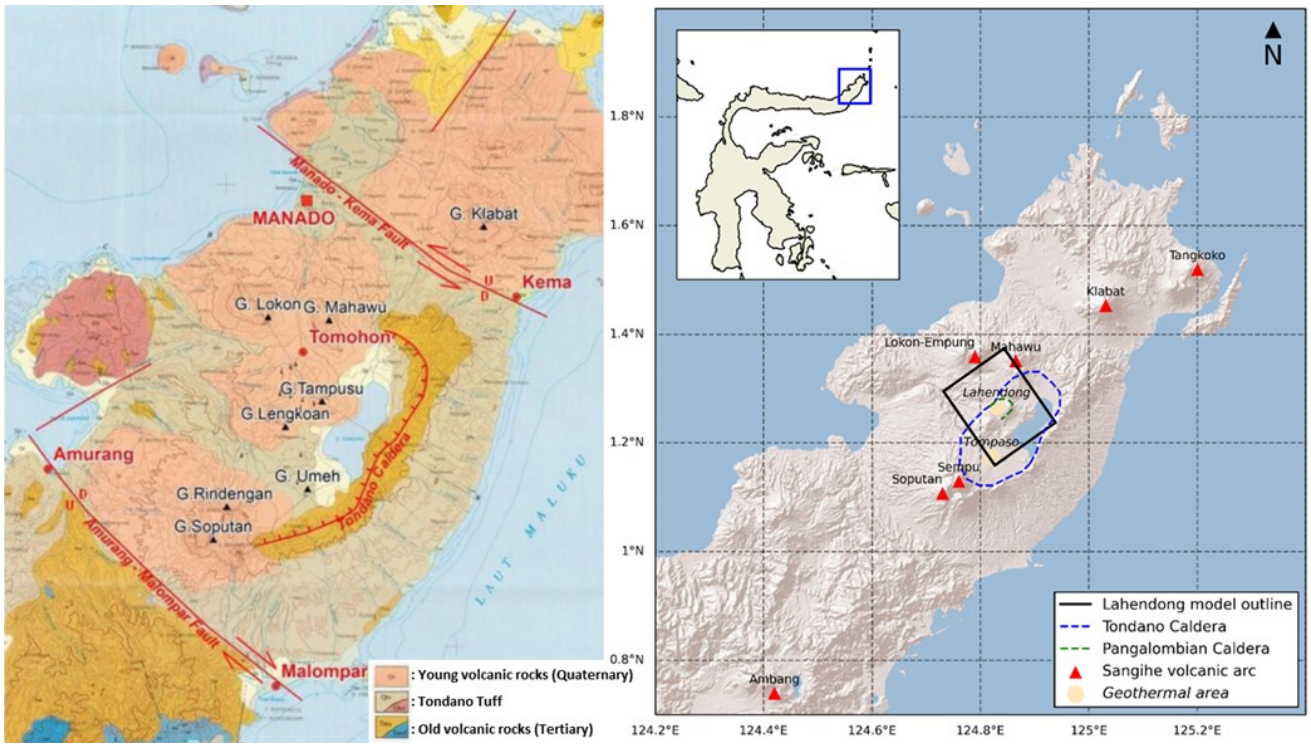

Figure 1: Regional location and geological context of the Lahendong Geothermal Field within the Minahasa peninsula with the new numerical model boundaries shown (modified from Effendi and Bawono, 1997).

The multidisciplinary project team included geoscientists, engineers, analysts and managers from each of the organisations. The project successfully achieved its objectives through close collaboration and an inclusive, transparent approach. The updated conceptual model, the updated Leapfrog digital conceptual model and the new numerical model not only provided an appropriate framework for carrying out the resource assessment – they are also invaluable tools for ongoing studies of the LGF. Details of the main stages in the project and the resulting models are discussed in the following sections.

2. CONCEPTUAL MODEL

2.1 Geological and structural model

The Lahendong area is influenced by the subduction of the Molucca Sea Plate beneath the Celebes Sea Plate, which induced several volcanic centres (Soputan, Mahawu, Klabat, etc.) oriented along a NNE-trending chain associated with the so-called Minahasa Compartment, resulting in NE-SW and NW-SE strike orientations and dominant permeable fractures in NE-SW directions (Sardiyanto et al. (2015)). The Tondano Caldera is ~20 km wide and extends for ~30 km along its north-south long axis. Pyroclastic and tuff deposits covering the Minahasa-Sangihe area are inferred to be Late Miocene or Early Pliocene age and are related to the initial Tondano Caldera collapse. The Tondano volcanic stratigraphy is classified through Pre-Tondano Unit, Tondano Unit and Post-Tondano Unit (Sumintadireja et al. 2001, Siahaan et al. 2005).

The Pre-Tondano Unit is associated with thick deposits of mid-Miocene to Pliocene andesite lavas, and pyroclastics breccia with lenses of volcano-sedimentary layers, containing carbonates and fossiliferous deposits. This unit is presumably associated with the inferred ancient caldera eruption that formed the original Old Tondano Caldera. The Tondano Unit is associated with the subsequent volcanism that occurred during the formation of the Tondano crater. It consists of a 180 m to 400 m thick layer of porphyritic, pyroxene-plagioclase andesitic lava and lapilli tuff-breccia and ignimbrite of rhyo-dacitic composition.

The youngest Post-Tondano unit is inferred from mid-Pleistocene volcanic events at Mt. Lengkoan, Pangolombian Caldera, Mt. Kasuratan, Mt. Tampusu and Linau hydrothermal-volcanic crater. The Post-Tondano Unit is encountered at the shallowest part of the Lahendong geothermal system, and is characterized by basaltic andesite to andesite lava and pyroclastics rocks, including andesite breccias. Intrusive microdiorite dikes are reported to have been intersected by LHD-5.

Within the large Tondano Caldera, the Lahendong Geothermal Field is located within the smaller, ellipsoidal Pangolombian Caldera (5 km long and 3.5 km wide) that formed approximately 450,000 years ago (Utami et al. 2015). Several young quaternary volcanic centres are related to the Pangalombian Caldera and constitute potential heat sources for Lahendong (i.e., Mt Kasuratan, Mt Tampusu, Linau Crater and Mt Lengkoan). Figure 2 shows 17 fault structures included in the digital conceptual model and implemented in the numerical model.

The area is influenced by two collapse structures: Pangalombian Caldera and Linau Crater. The Linau Crater hosts a lake containing meteoric water. Wells LHD-23, 24, 28, 29 track beneath the Linau Crater. They have high temperatures and contain magmatic-acid fluid (pH 1-2, high SO_4-waters), but exhibit low permeability, limiting lateral fluid low. The Leilem 2 Fault forms a boundary between the volcanic products from Mt Lengkoan, and Mt Kasuratan in the SE. The Tondangow 1 Fault divides the field into the North (Pangalombian) block with low temperature and moderate permeability, and South (Kasuratan) block with higher temperature and lower permeability.

The hydrology of the Lahendong geothermal system is inferred to be strongly controlled by several faults which compartmentalize the system. This is corroborated by geographical differences in the geochemistry of the sub-reservoirs (Brehme et al. 2014; 2016 a). The faults can act as barriers due to sealing processes or major pathways for the geothermal fluids (Utami 2011). Steam-heated and fumarolic surface features associated with faults occur within the central faulted area, while bicarbonate-rich springs are observed at the margins of Lahendong (Utami 2011). Fluid recharge into the reservoir was discussed at a conceptual level in Widagdo et al (2005).

2.3 Geophysics, geochemistry and alteration model

From joint MT-gravity inversion, a higher density region coinciding with anomalously high resistivity at the core of the high temperature reservoir occurs at depths between -1000 mRL and -2000 mRL. This may reflect densification of host rocks by silica deposition infilling pores. Alternatively, the anomaly could result from a denser intrusive rock mass under the reservoir (i.e., below drilled depths). The intrusive could be a potential heat source. A wide distribution of micro-seismic events is located at depths to -3000 mRL, suggesting the presence of high-temperature, mostly ductile conditions below the depth of -3000 mRL. However, the conceptual model needs to account for some deeper penetrating fractures that can bring hot recharge fluids into the productive reservoir.

The 3D inversion of Magnetotelluric (MT) data from Lahendong shows a simple propylitic resistive dome of 20-60 ohm.m encapsulated by a conductive clay cap of less than 10 ohm.m (Raharjo 2010). The shallower part near the peak of the dome is below the acidic Lake Linau and situated about 500 m below the surface. It extends to the south at greater depth with a steeper side to the north.

Hydrothermal alteration at Lahendong has resulted from subsurface fluid-rock interactions leading to mineral deposition in veins and pores in the host rocks. Down to near sea level, the dominant secondary minerals are calcite, quartz and hematite (Utami 2011). Below sea level, epidote and other calc-silicate minerals are markers of high subsurface temperatures created by upflows. A large and deep magmatic heat source for the geothermal system is inferred below LHD-5 with high-temperature mineral indicators below 225 masl. Explicit inclusion of the alteration zones in the model accommodates heterogeneity in the structural properties of the reservoir. The inferred conductive clay cap is based on 3D MT data, temperature data and feed zone elevations. These features are included in the digital conceptual and reservoir model.

2.3 Heat source

Previous studies located the heat source in the southern part of the Lahendong area and suggested heat migrates to the NW through fault-controlled pathways (Sumintadireja et al. 2001). Beneath Lake Linau, a magma chamber is inferred from occurrence of acidic water resulting from H_2S degassing (Brehme et al. 2014). Recently it has been suggested that the primary heat source is located at the centre of Linau, Kasuratan and Lahendong, with a minor heat flow at Pagolombian (Atmojo et al 2015). A heat source beneath Mt. Lengkoan and Mt. Kasuratan arising from magma cooling has also been suggested (Siahaan, 2005).

The magmatic signature is significant in wells LHD-47, LHD-48 and LHD-49 and a heat source next to Lake Linau is inferred from the production data in LHD-23 and LHD-28. Gas compositions show indications of a magmatic fluid input, particularly in the Lake Linau area, and from wells LHD-23 and LHD-28. The location of hot upflows is indicated by wells with temperatures above 300°C (and sometimes up to 350°C, e.g., LHD-13 and LHD-47).

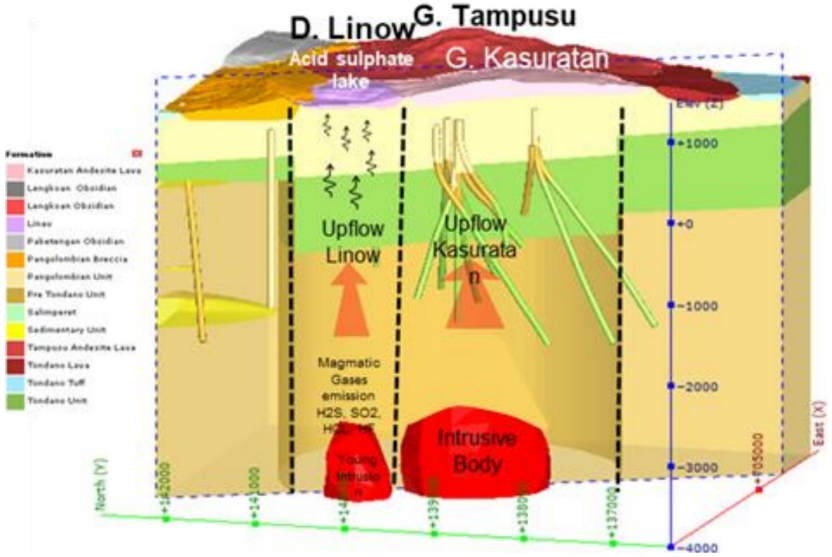

Figure 2: Cross-section showing the conceptual model of the Lahendong Geothermal Field (adapted from Prasetyo et al., 2021).

2.4 Leapfrog Digital Conceptual Model Update

Leapfrog digital conceptual models have become increasingly common tools for representing, analysing and interrogating geothermal conceptual models. Leapfrog allows users to visualise the conceptual model easily in 3D and enables better interaction between all the stakeholders in a geothermal development (O'Sullivan et al., 2019; Popineau et al., 2018). Leapfrog has the advantage that it can be used to tightly couple the digital conceptual model to numerical model through an integrated modelling framework that has been developed at the University of Auckland (O'Sullivan et al., 2019; Popineau et al., 2018).

However, before developing a numerical model coupled to the Leapfrog digital conceptual model, the Lahendong Leapfrog model needed to be updated to include the latest conceptual model information and it needed to be revised so that it was consistent with our integrated modelling framework. Three main revisions were made:

- The geological model was extended laterally so that it covered the entire numerical model.
- The structural model was adapted, explicitly including more faults that can act as pathways and barriers for fluid flow.
- An inferred model of the shallow conductor (clay-cap) was included.

The lateral extent of the new Leapfrog model compared with the previous version is shown in Figure 3. The plots in Figure 4 show 3D views of geology, subsurface structures and alteration zone in the updated digital conceptual model.

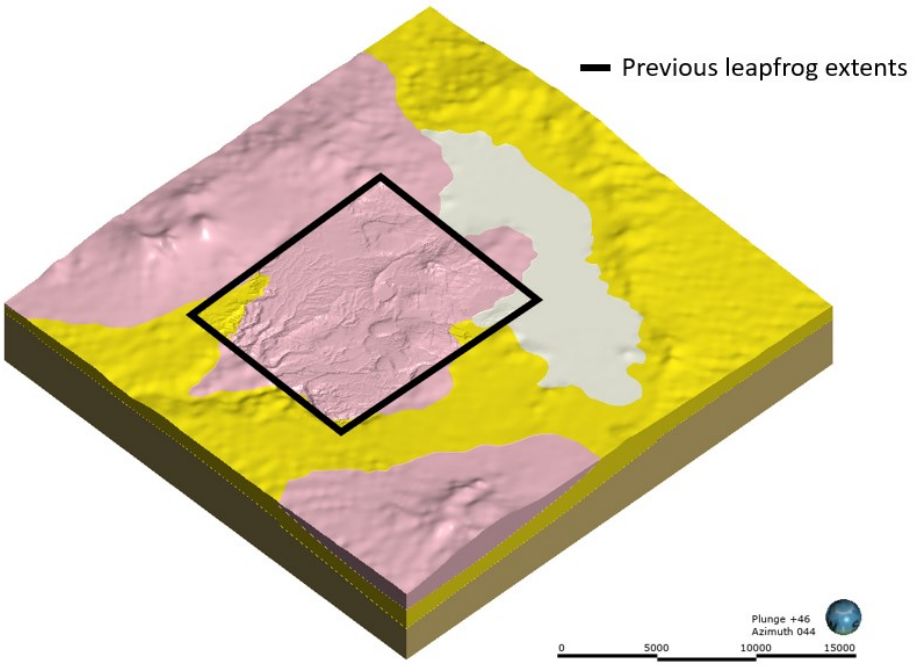

Figure 3: The new Leapfrog geological model. The extent of the previous model is shown in black.

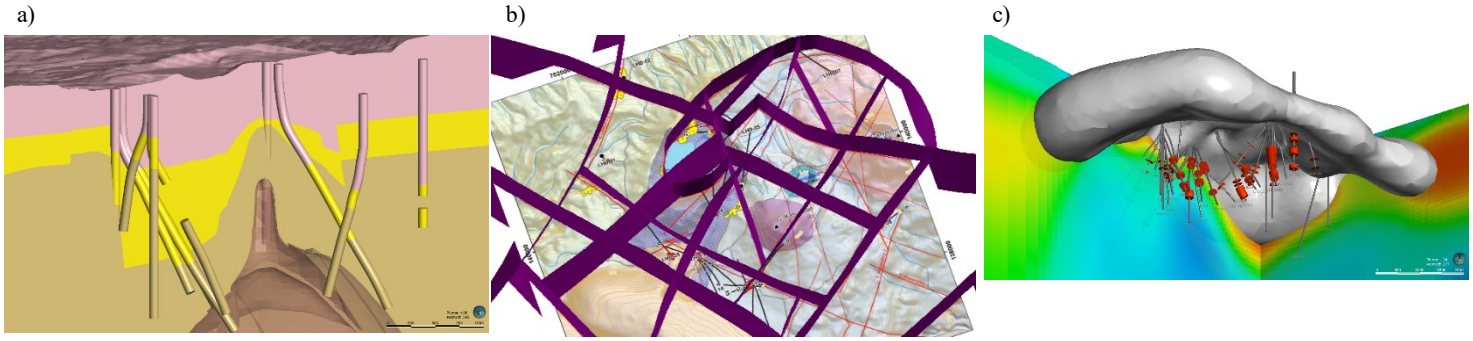

Figure 4: (a) A cut-away cross-section of the new Leapfrog geological model. (b) The new structural model shown above a map of the LGF. (c) The interpreted clay-cap viewed from below (grey) shown with MT resistivity slices and production wells with feedzones shown in red.

3. NUMERICAL MODEL REVIEW

An important stage in the project was to review the previous numerical models of the LGF and determine if the current model was appropriate for carrying out a resource assessment of the system. Our review is summarised below including discussion of the limitations of the existing model and our decision to develop a new numerical model. The setup of the new numerical model, coupled to the Leapfrog digital conceptual model, is presented in the following section.

3.1 Previous numerical models

Various numerical models of Lahendong have been developed in the past focusing on the natural state temperatures in the field (Yani 2006, Sumantoro et al. 2015, Koestono et al. 2010). Inverse modelling with PEST and iTOUGH2 has also been used to refine the match of the model (Prasetyo et al. 2016). Later, refinements of the grid and the implementation of an alteration model based on available resistivity data led to better constraints on the permeability field, with again no production data included (Prasetyo et al., 2016).

A recent numerical model of the Tompaso sector of the Lahendong geothermal system produced a good representation of the natural state (Lesmana et al., 2019, 2021). The model contained 38,502 blocks, covering an area of 39 km^2 with 17 layers extending from ground surface to -2400 masl. The top of the model follows the topography but the EOS1 (all water) equation of state is used, and so no unsaturated zone was included at the top of the model. Temperature data from eight wells in the Pinabetengan area (LHD-26, LHD-27 and LHD-30 to LHD-35) and two wells in the Tempang area (R1 and R2) were used for calibration of the natural state model.

Brehme et al. (2014, 2016a) developed a conceptual model for the large-scale behaviour of the greater Lahendong area in terms of upflows controlled by the local and regional faults. Based on the conceptual model, Brehme et al. 2016b set up a large-scale, 2D numerical model of the anisotropic permeability distribution on a vertical SW-NE slice through Lahendong. The FEFLOW, liquid-water-only numerical model, matched the measured temperatures and pressures at selected observation points in a few wells.

The importance of high permeability flow pathways at Lahendong has also been inferred from tracer tests performed in LHD-7 (Prabowo et al. 2015). A thermo-hydro-mechanical simulation was also set up, and aimed at capturing the key processes in Lahendong (Qarinur et al. (2020), but did not achieve very good results.

The previous PGE model of Lahendong was implemented in TOUGH2 via the Petrasim interface. It consists of 13,500 model blocks, with 900 columns and 15 layers (including an atmospheric layer). The model extends vertically from 900 masl to -2500 masl. Figure 5a shows the lateral extent of the grid while Figure 5b shows the vertical structure of the model. Figure 5a includes well tracks and the caldera boundary.

From **Error! Reference source not found.** we can see that the top of the previous PGE model is flat, and boundary conditions set for the model do not allow for topographical influences on the flows. The plots show the extent of the previous model is sufficient. However, the calibrated natural state model gave only a reasonable match to downhole temperature profiles and there was no production history model.

a)

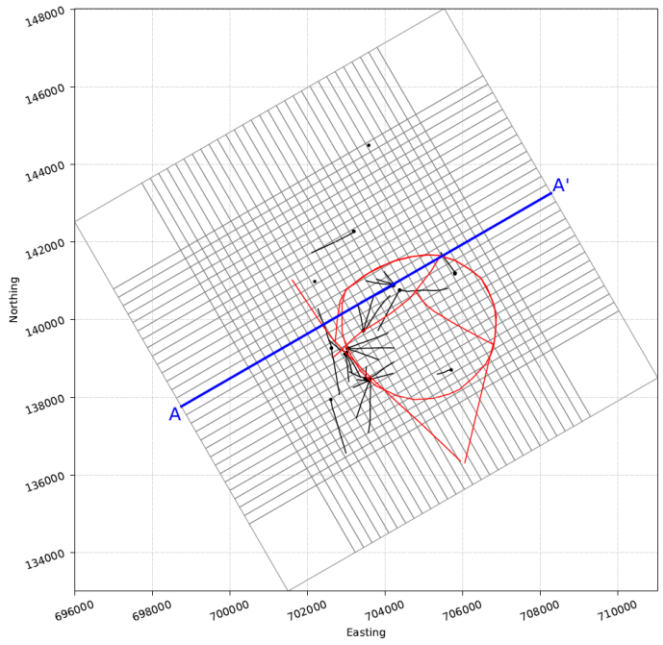

b)

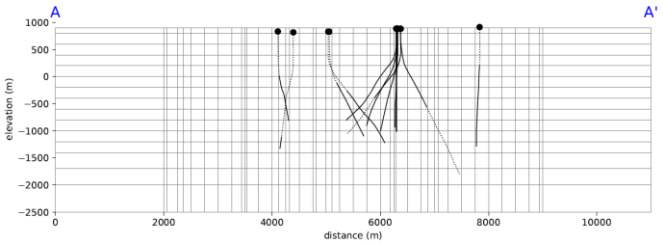

Figure 5: (a) Plan view of the previous PGE reservoir model grid with structures included in the model are over laid in red. (b) Cross-section through the model showing the layer structure and a selection of production well tracks.

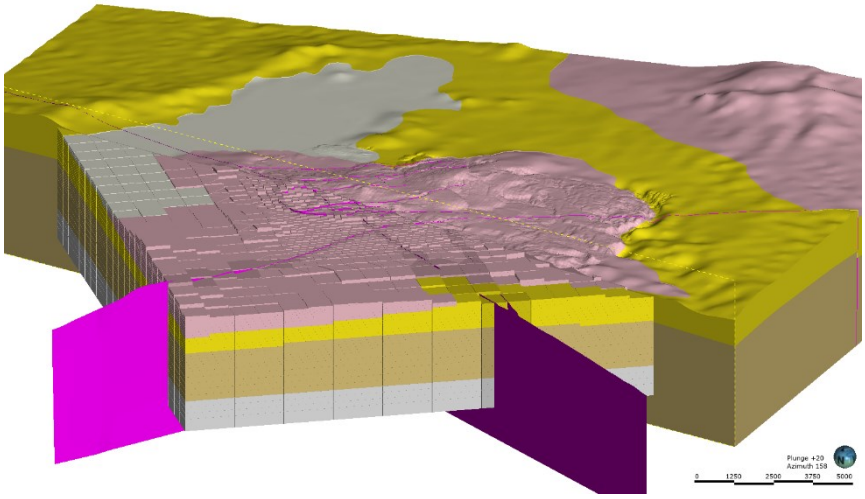

Figure 6: A comparison of the Leapfrog digital conceptual model (top half) and the coupled numerical model (bottom half). Magenta surfaces indicate structures in the digital conceptual model with the corresponding numerical model blocks shaded.

4. NUMERICAL MODEL DEVELOPMENT

Based on the limitations of the previous model as discussed above, a new numerical model was developed. In this section we outline the coupling of the new numerical model to the Leapfrog digital conceptual model and present the model setup.

4.1 Creation of the numerical model

In the workflow used in this project we coupled the Leapfrog digital conceptual model (including the geology, structural framework, and hydrothermal alteration) directly to a numerical model using our integrated modelling framework (O'Sullivan et al., 2019; Popineau et al., 2018). This means that the numerical model explicitly represents the best understanding of the geology and geophysics structure of the field. Faults, structures and hydrothermal alteration are represented explicitly with rock-types which allow the properties of these features to be represented and provides heterogeneity to allow the model to be appropriately calibrated to reservoir engineering data. Figure 6 shows a comparison of the Leapfrog digital conceptual model and the coupled numerical model.

4.2 Model grid

The grid selected for the new numerical model is shown in Figure with well tracks superimposed and the resistivity boundary included. A SW-NE vertical slice through the model is shown in Figure . There were several criteria which determined the design of the new grid:

- The grid is orientated at an angle of 35 degrees (anti-clockwise) from north to align the model blocks with major flow pathways.
- The grid uses local refinement to create its highest resolution with blocks that are small enough (200 m x 200 m) to provide reasonable resolution.
- A large area around the hot reservoir is included to allow cold recharge to be represented in the model.
- The fine grid covers the full resistivity boundary.
- The top of the model is at ground surface and thus follows the topography (see Figure). Thus, the model includes the shallow unsaturated zone and has higher resolution layers in these elevations.
- The base of the model is set at -3000 masl. This is 1200 m below the bottom of the deepest well.

The new model has 60,094 blocks, with 41 layers covering an area of 18.5 km x 15 km.

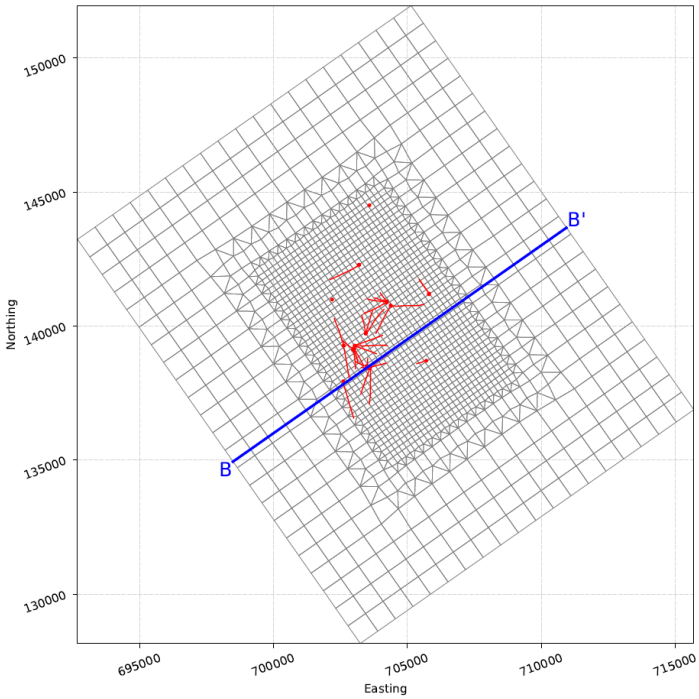

Figure 7: Plan view of the model grid showing the well tracks (red). B-B' defines a cross-section used in subsequent figures.

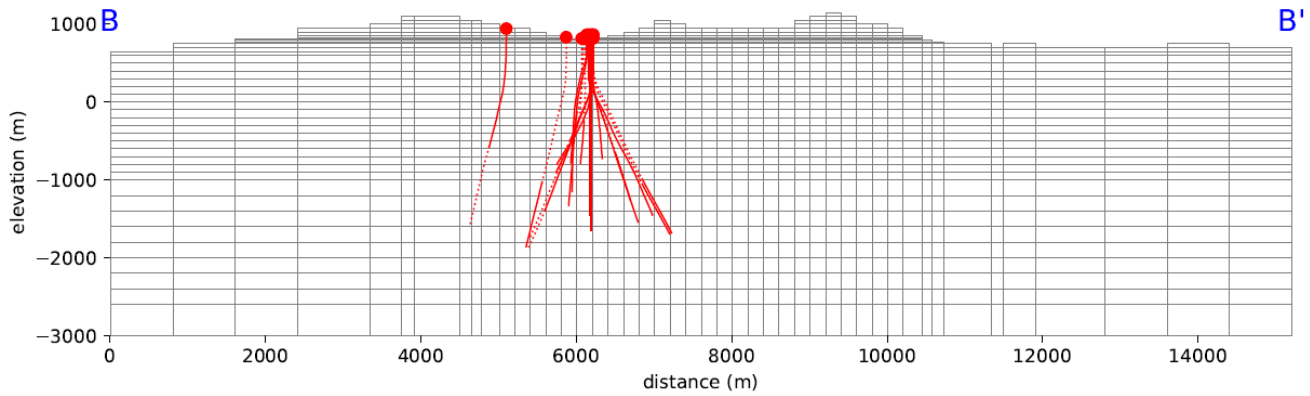

Figure 8: SW-NE vertical slice (B-B' as defined in Figure) through the model grid showing well tracks and topography

4.3 Boundary conditions

In this section we discuss the boundary conditions used in the new model.

Top boundary

The model represents the geothermal system to the surface using an air/water equation of state. This means that most surface blocks are connected to the atmosphere, with a boundary condition of constant pressure and temperature of 1.01325 bar and 24 °C, respectively. The exception to this is where the surface blocks are underneath a body of water (such as Lake Linau). These surface blocks are shown in Figure 9. In this case the pressure boundary condition is calculated based on the hydrostatic pressure from the depth of the body of water. Lake Linau was assumed to have an average depth of 5m and an average temperature of 24 °C. Lake Tondano was assumed to have a depth of 10 m and an average temperature of 24 °C.

In the Lahendong model we also explicitly represent rainfall. We assumed a constant rainfall of 1800 mm/year throughout the simulation with an infiltration rate of 10 % and a temperature of 24 °C. This is represented by mass source terms in the surface blocks with an appropriate enthalpy. Rain is not input to blocks that are beneath the lakes.

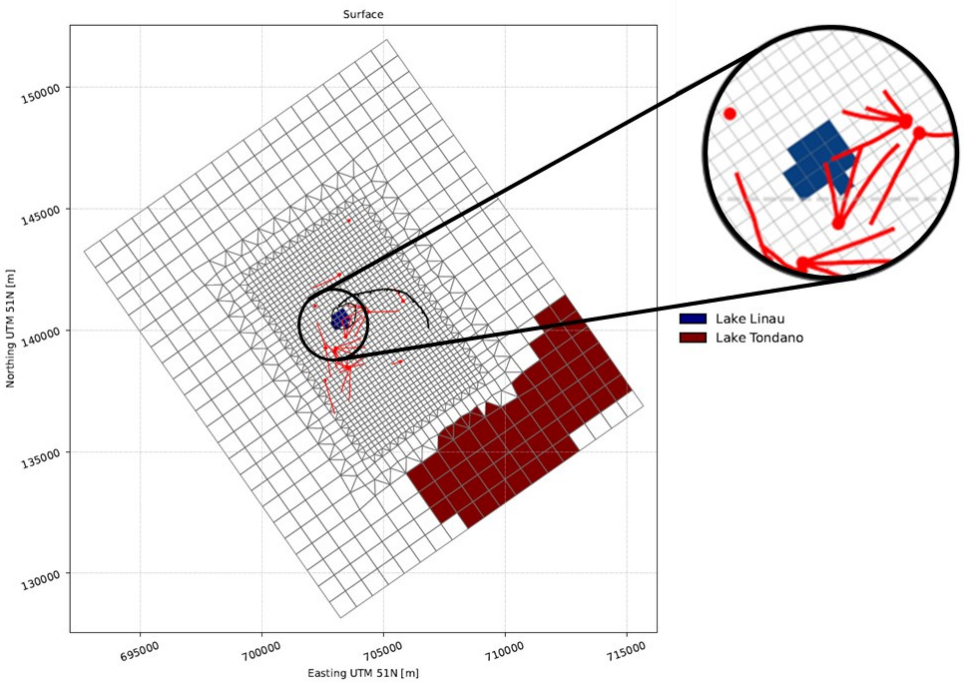

Figure 9: Blocks in the top layer of the model underneath Lake Linau and Lake Tondano

Side boundary

All sides are treated as no-flow boundaries for both heat and mass. This is a reasonable assumption as the boundaries are well away from the edges of the reservoir.

Bottom boundary

The boundary conditions at the bottom of the system represent two things:

1. A mass upflow representing a convective plume of hot water coming from deeper than the base of the model
2. A background conductive heat flow.

To represent the conductive heat flow, all blocks at the base of the model have an input of a constant heat flux of 80 mW/m^2. Mass source terms are added to some blocks in the base of the model to represent the hot upflow. Determining the location, mass flow and enthalpy of these source terms is part of the calibration process. Figure 10 shows the location and magnitude of these upflow source terms in the calibrated model. In general, upflows are placed on fault structures to maintain consistency with the conceptual understanding of the upflow occurring on preferential vertical permeability pathways.

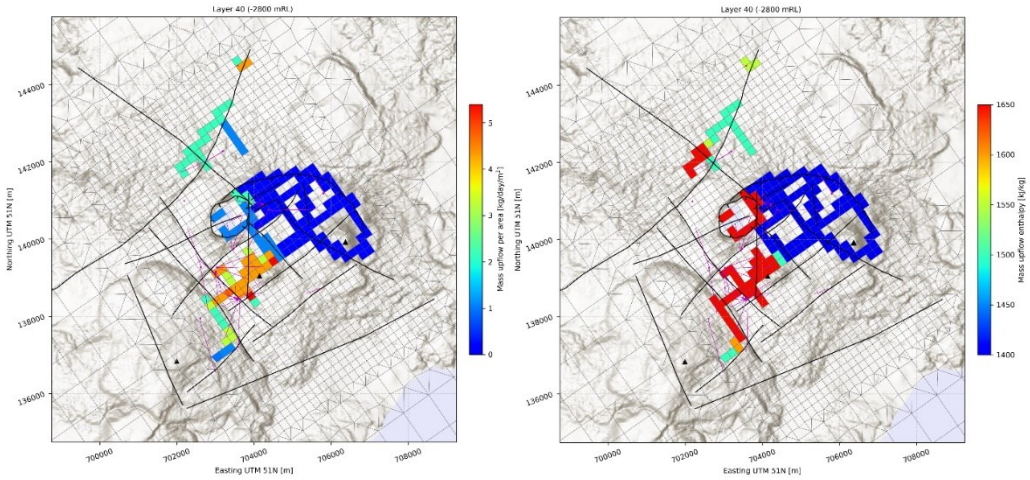

Figure 10: Mass upflows set at the bottom of the model (left). Enthalpy of the upflows at the bottom of the model (right). The surface traces of the faults are shown with the black curves.

4.4 Geothermal simulators

The new numerical model is set up to be run in either AUTOUGH2 (Yeh et al., 2012), a local variant of the industry-standard simulator TOUGH2 (Pruess et al., 1985), or in Waiwera (Croucher et al., 2016, 2017, 2018, 2020; O'Sullivan et al., 2017), a highly parallelised, open-source simulator developed by the University of Auckland and GNS Science. Running the model interchangeably using both simulators leverages the power of Waiwera for fast calibration times and rapid model development while retaining the confidence that TOUGH2 provides as the industry-standard simulator

5. NUMERICAL MODEL CALIBRATION

5.1 Natural state calibration

The large-scale objectives of natural state calibration were as follows:

- To achieve a maximum temperature at the bottom of the reservoir of ~ 350 °C
- To represent the main flow directions (upflow, outflow, inflow) detailed in the conceptual model
- To broadly represent interpreted natural state temperatures and pressures
- To achieve an appropriate match to natural surface features

To achieve these aims the following quantities were found to be the most influential parameters:

- Base temperature (enthalpy of mass up flow)
- Magnitude of mass upflows at the base of the model
- Average vertical permeability in the reservoir
- Average horizontal permeability in the reservoir

The calibrated values for the magnitude and enthalpy of the mass upflows are presented in Figure 10 and an example of the vertical permeability distribution in a layer of the calibrated model is shown in **Error! Reference source not found.**. The calibrated model gives the following insights into the heat source and the permeability structure of the LGF:

- The different compartments of the system are likely to have different upflow characteristics (enthalpies and flow rates), in line with the conceptual model analysis
- Outside the reservoir vertical permeabilities are very low (dark blue in **Error! Reference source not found.**)
- Background permeabilities are low beneath the reservoir (light blue in Figure 11)
- Several of the NW trending faults are likely to have high vertical permeability (orange and red in **Error! Reference source not found.**)
- Several of the NE trending faults are likely to have high vertical permeability (orange and red in **Error! Reference source not found.**)
- Highest vertical permeabilities are likely to be found on faults above the diorite intrusion and at the intersection of faults

In general, the match of the calibrated natural state model results to the measured data is good. There are mismatches in some wells but there is also some uncertainty in the temperature data since downhole temperature measurements were made long after production started at the LGF and there are some inconsistencies between measured downhole temperatures and measured production enthalpies. Examples of the downhole temperature plots from the calibrated model against measured data are shown in **Error! Reference source not found.**.

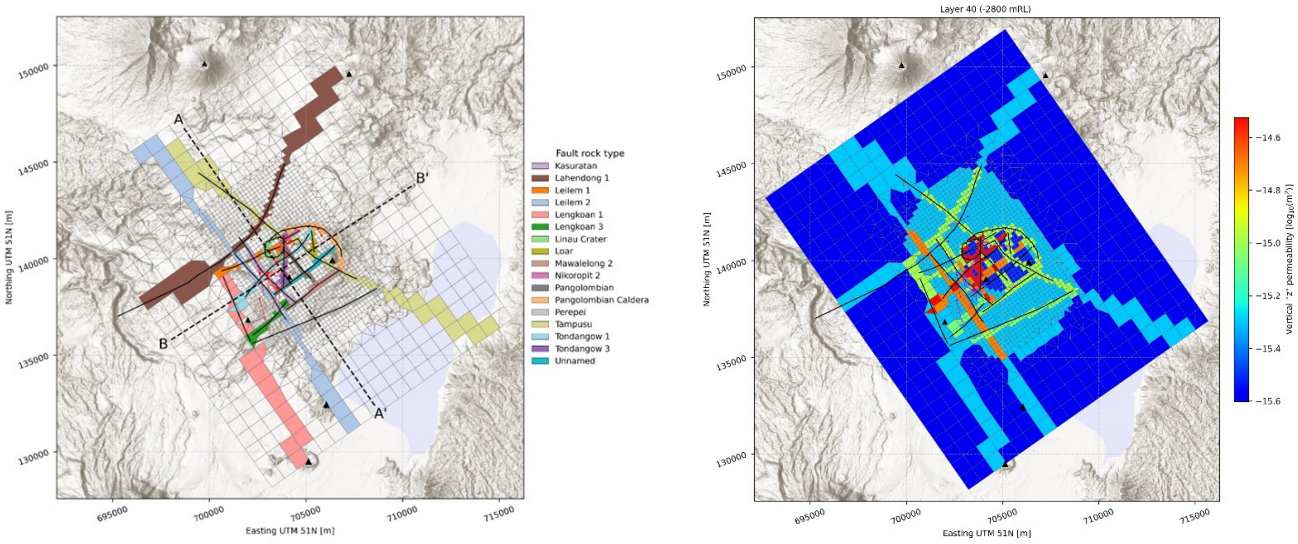

Figure 11: Left) Faults implemented in the numerical model. Right) Vertical permeability distribution at the base of the model. The surface topography background is superimposed.

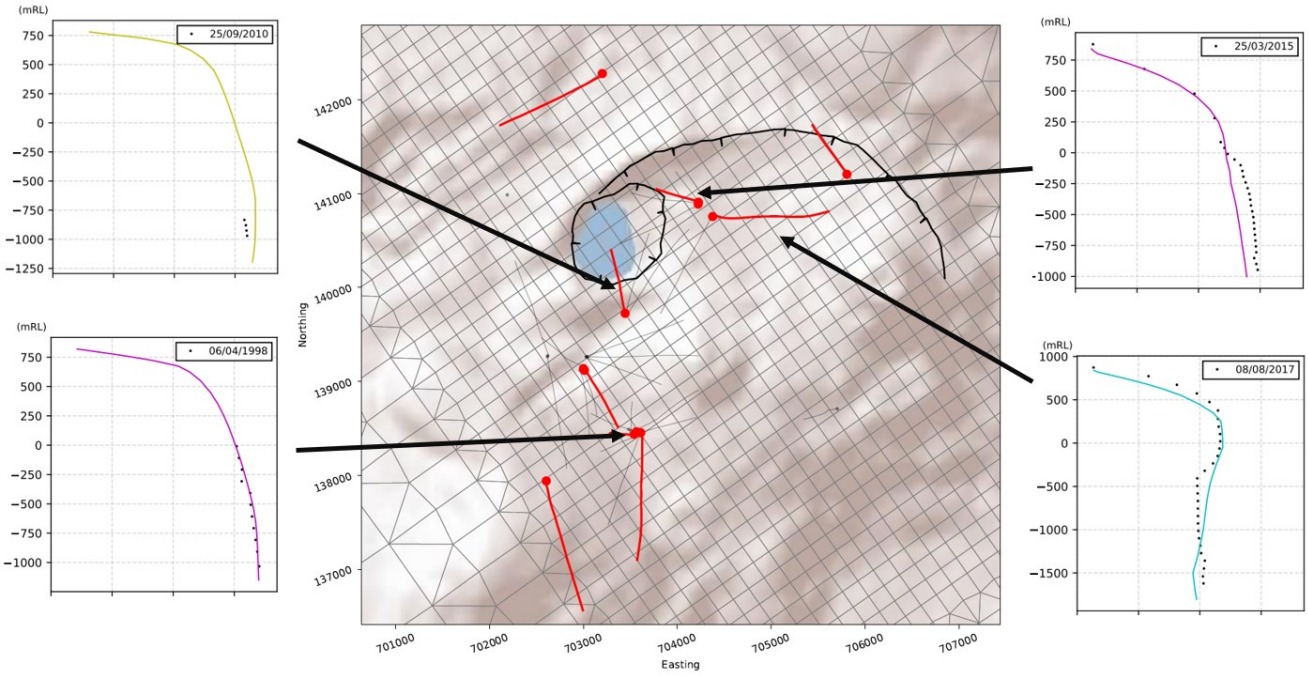

Figure 12: Downhole temperature vs elevation for selected wells including their location in the LGF. Model results are given as lines and measured data as black symbols.

Temperatures on vertical slices through the calibrated model (defined in Figure 10) are given in **Error! Reference source not found.** showing the large-scale convection in the different compartments at the LGF.

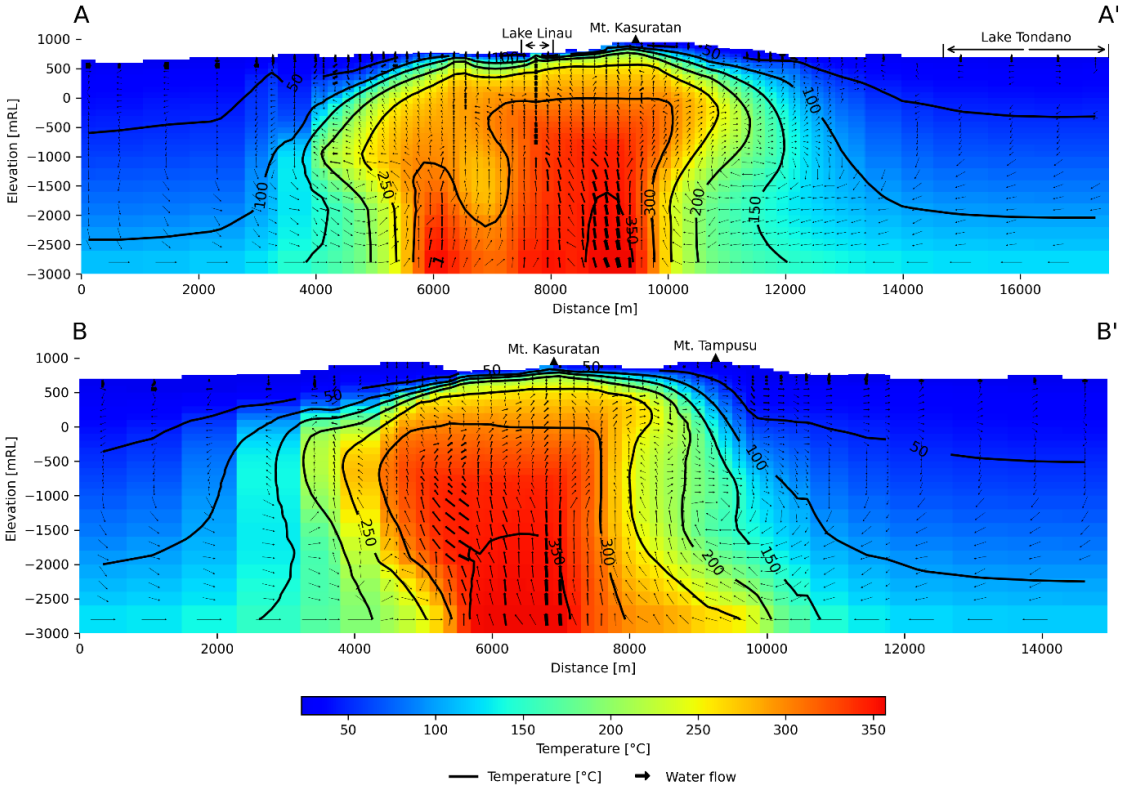

Figure 13: Top) NW-SE slice and Bottom) SW-NE slice in the model with the temperature distribution and water mass flow. The locations of the slices A-A' and B-B' are defined in Figure 11.

5.2 Production history calibration

The production history model was calibrated by adjusting local permeability and porosities to match measured transient pressure and enthalpy data. For the production history simulation a dual porosity model was used. In a dual porosity model, high-permeability, low-volume fractures are embedded in a low permeability matrix. In TOUGH2 this dual continuum is represented by the MINC system (Pruess and Narasimhan, 1985) with each block of the single porosity model partitioned into a fracture block and one or more matrix blocks. The parameters used are shown in Table .

Table 1: Dual porosity parameters used in the production history model

Parameter	Value
Number of matrix blocks	2 (20% and 75%)
Volume fraction of fracture blocks	5%
Fracture spacing	25 m
Fracture planes	3
Permeability of matrix	1.0E-16 m^2
Porosity of matrix	6.3%, 16.8% or 22.1%
Permeability of fractures	variable
Porosity of fractures	variable

Overall, a good match was achieved between the production history model and the measure transient pressure data. A typical page of plots is shown in Figure 14 where the match to the data for the pressure decline and the enthalpy response for the well is good. A similar high quality of match to the data for pressure decline and enthalpy response is achieved for most wells. In several wells the model enthalpies are more variable than the measured data. This may be a result of a high level of uncertainty in the individual well production flow rates.

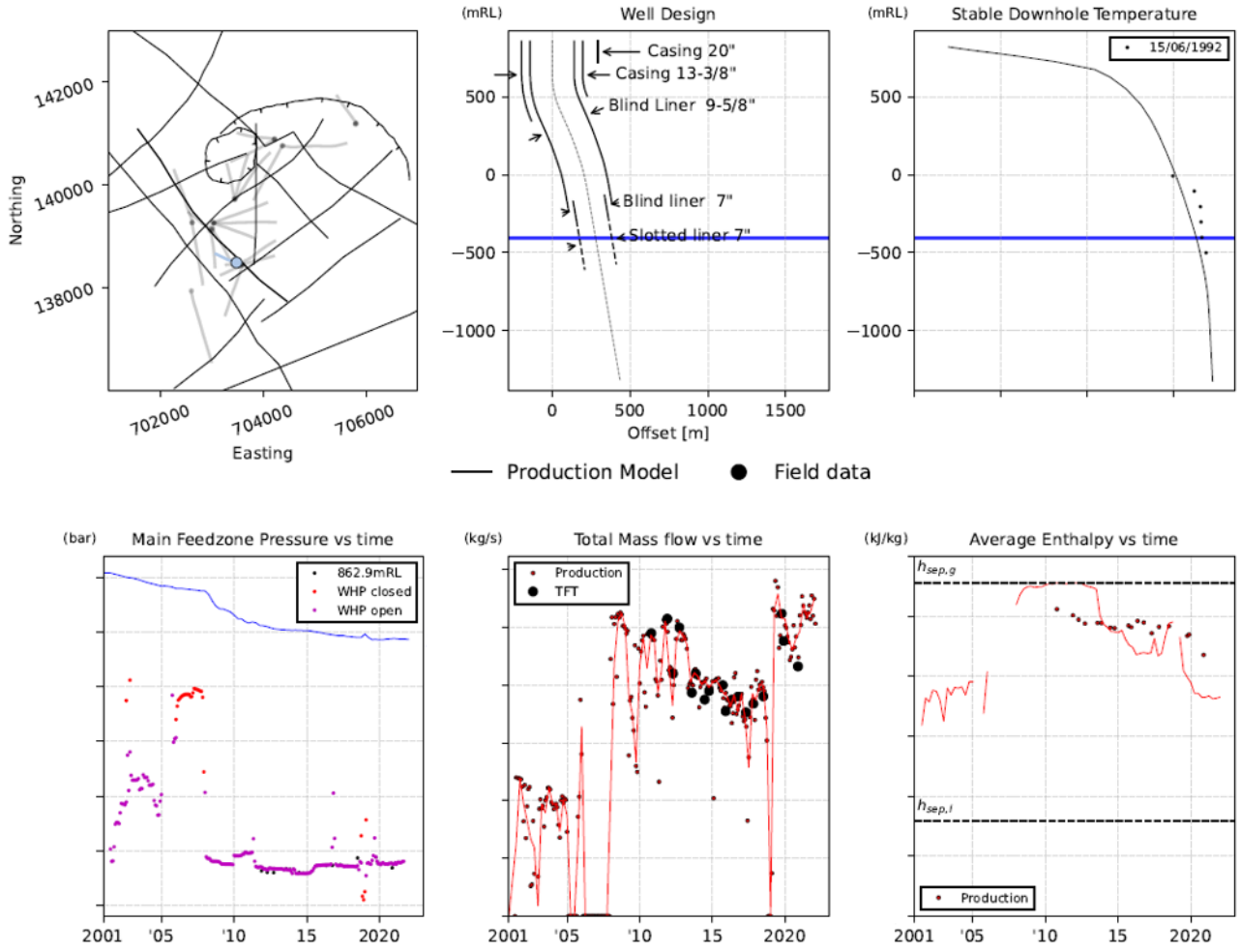

Figure 14: Typical calibrated production history model results for a production well. Model results shown as solid lines and measured data as symbols.

5. MODEL FORECASTS

The calibrated production history model has been used to make a range of forecasts about the future behaviour of the LGF. Scenarios investigated so far include:

- Targeting future make-up wells
- Scheduling make-up wells
- Assessing the resource potential through various make-up well scenarios

The future scenarios are all run using the same dual porosity model set up as the production history model. However, existing production wells and future make-up wells are represented by wells on deliverability with properties determined using detailed wellbore modelling. Model results from the future scenarios are visualised through standardised sets of reports but can also be easily loaded into Leapfrog to generate 3D views and animations to help understand and communicate the findings of the modelling studies.

Numerical modelling of geothermal systems is affected by many types of uncertainty. These include, but are not limited to, uncertainty in the measured data, uncertainty in the unknown structure of the subsurface, uncertainty in the future operation of the resource and uncertainty in the model parameters.

The numerical modelling project of the LGF includes all these uncertainties and quantifying the level of uncertainty in the forecasts from the new model was outside the scope of this project. However, well-established geothermal modelling practices were used to develop the new model, and therefore it is likely to produce accurate forecasts.

6. CONCLUSION

This paper discusses a new modelling study of the Lahendong Geothermal Field carried out by a multidisciplinary team made up of members from PT. Pertamina Geothermal Energy, the Geothermal Institute at the University of Auckland, Geoenergis Solusi Indonesia,

and independent New Zealand geothermal experts. The project successfully achieved its objectives through close collaboration and an inclusive, transparent approach.

A review and update of the conceptual model of Lahendong were conducted resulting in an updated digital conceptual model, implemented in the Leapfrog Geothermal software. The new Leapfrog model was developed using well-established conceptual modelling techniques and is consistent with the data provided. It covers a larger area and has a more detailed representation of the geothermal system than the existing Leapfrog model used by PGE.

Limitations in the existing numerical model required a new numerical model to be set up. The new numerical model was created following well-established numerical modelling techniques that ensure the model is consistent with the conceptual model and capable of accurately representing the behaviour of the Lahendong Geothermal Field over time.

The key differences between this new numerical model of Lahendong and the existing PGE model are:

- It covers a larger area than the PGE numerical model.
- It extends vertically up to the ground surface, thus following the topography and including the unsaturated zone in the model allowing for a better representation of shallow pressures.
- It extends down to a base at -3000 masl, providing a better representation of the deeper production feedzones.
- It is tightly coupled to the geological and geophysical data in the digital conceptual model ensuring consistency.
- It is a dual-porosity model explicitly modelling flow in fracture pathways enabling a more accurate representation of pressure and enthalpy changes over time.

The new numerical model was calibrated against the measured data provided by PGE using the industry-standard approach. The natural state model was calibrated against all the available downhole temperature profiles and then the production history model was calibrated against the available pressure decline and enthalpy response data. A satisfactory match to the temperature profiles and a very good match to the pressure decline and enthalpy response data were obtained.

The state of model calibration achieved is good and therefore, we are confident that the model provides a good representation of the Lahendong Geothermal Field and is appropriate to use for forecasting.

7. ACKNOWLEDGEMENTS

The authors would like to thank PT. Pertamina Geothermal Energy for permission to publish this work.

REFERENCES

Atmojo J. P, Widarto, D., S., Kamah, Y., Bramantyo, E.A.: Heat Source Movements in Lahendong Geothermal Field and Its Affect to The Reservoir Characteristics, Proceedings, World Geothermal Congress 2015 Melbourne, Australia, (2015).

Brehme, M., Moeck, I., Kamah, Y., Zimmermann, G., Sauter,M.: A hydrotectonic model of a geothermal reservoir – A study in Lahendong, Indonesia, Geothermics, 51, (2014), 228–239.

Brehme, M., Blocher, G., Cacace, M., Kamah, Y., Sauter, M., Zimmermann, G.: Permeability distribution in the Lahendong geothermal field: A blind fault captured by thermal–hydraulic simulation, Environ Earth Sci (2016a).

Brehme, M., Deon, F., Haase, C., Wiegand, B., Kamah, Y., Sauter, M., Regenspurg, S.: Fault controlled geochemical properties in Lahendong geothermal reservoir Indonesia Grundwasser – Zeitschrift der Fachsektion Hydrogeologie (2016b).

Croucher, A., OSullivan, M. J., O'Sullivan, J. P., Pogacnik, J., Yeh, A., Burnell, J., Kissling, W.: Geothermal supermodels project: An update on flow simulator development. Proc. 38th New Zealand Geothermal Workshop. Auckland, New Zealand. (2016).

Croucher, A. E., Osullivan, M. J., O'Sullivan, J. P., Pogacnik, J., Yeh, A., Burnell, J., Kissling, W.: Geothermal Supermodels project: an update on flow simulator development. Proc. 39th New Zealand Geothermal Workshop. Rotorua, New Zealand. (2017).

Croucher, A. E., O'Sullivan, J. P., Yeh, A., O'Sullivan, M. J.: Benchmarking and experiments with Waiwera, a new geothermal simulator. Proc. 43rd Workshop on Geothermal Reservoir Engineering. Stanford University, Stanford, California, USA. (2018).

Croucher, A., Osullivan, M.J., O'Sullivan, J.P., Yeh, A., Burnell, J., Kissling, W.: Waiwera: a parallel open-source geothermal flow simulator. Computers and Geosciences 141. https://doi.org/10.1016/j.cageo.2020.104529 (2020).

Effendi, A.C., Bawono, S.S.: Geologic Map of the Manado quadrangle, North Sulawesi, 1:250.000 scale, Geological Survey Indonesia, Bandung, (1997).

Hochstein, M.P., Sudarman, S.: History of geothermal exploration in Indonesia from 1970 to 2000, Geothermics, 37, (2008), 220–266.

Koestono, H., Siahaan E.E., Marihot Silaban, M., Franzson, H.: Geothermal model of the Lahendong Geothermal Field, Indonesia, Proceedings, World Geothermal Congress 2010 Bali, Indonesia, (2010).

Lesmana, A., Pratama, H.B., Ashat, A., Saptadji, N.M., Gunawan, F.: An updated conceptual model of the Tompaso geothermal field using numerical simulation, Proceedings, 41st New Zealand Geothermal Workshop Auckland, New Zealand (2019).

Lesmana A. Pratama H.B., Ashat A., Saptadji N. M.: Sustainability for geothermal development strategy using a numerical reservoir modelling: a case study of Tompaso geothermal field, Geothermics, Volume 96, (2021).

O'Sullivan, J. P., Croucher, A.E, Popineau, J., Yeh, A., O'Sullivan, M.J.: Working with multi-million block geothermal reservoir models. Proc. 44th Workshop on Geothermal Reservoir Engineering. Stanford University, Stanford, California, USA. (2019)

O'Sullivan, J.P., Croucher, A.E., Yeh, A., O'Sullivan, M.J.: Experiments with Waiwera, a new geothermal simulator. Proc. 39th NZ Geothermal Workshop, Rotorua, New Zealand. (2017)

Popineau, J., O'Sullivan, J.P., O'Sullivan, M.J., Archer, R., Williams, B.: An integrated Leapfrog/TOUGH2 workflow for a geothermal production modelling. Proceedings, 7th African Rift Geothermal Conference (ARGeo). Kigali, Rwanda. (2018).

Prasetyo, F., O'Sullivan, J., O'Sullivan, M.: Inverse modelling of Lahendong geothermal field, Proceedings, 38th New Zealand Geothermal Workshop Auckland, New Zealand (2016).

Prasetyo, Imam M., Sardiyanto, Dian Larasati, and contributors to EGRE Geosciences team (2021) 'Lahendong Geothermal Field Conceptual Model Update' Confidential Pertamina Internal Report September 2021.

Prabowo, T., Yuniar, D.M., Suryanto, S., Silaban, M.: Tracer Test Implementation and Analysis in Order to Evaluate Reinjection Effects in Lahendong Field , Proceedings, World Geothermal Congress 2015 Melbourne, Australia, (2015).

Pruess, K. and Narasimhan, T.N. A: Practical Method for Modeling Fluid and Heat Flow in Fractured Porous Media, Society of Petroleum Engineers Journal, 25(1), (1985), 14-26.

Pruess, K., Oldenburg, C., Moridis, G.: TOUGH2 User Guide version 2 (2012).

Qarinur M., Ogata, S., Kinoshita N., Yasuhara, H.: Predictions of Rock Temperature Evolution at the Lahendong Geothermal Field by Coupled Numerical Model with Discrete Fracture Model Scheme, Energies (2020).

Raharjo, I.B., Maris, V., Wannamaker, P.E., Chapman, D.S.: Resistivity Structures of Lahendong and Kamojang Geothermal Systems Revealed from 3-D Magnetotelluric Inversions, A Comparative Study, Proceedings, World Geothermal Congress 2010 Bali, Indonesia, (2010).

Sardiyanto, N.S., Prasetyo, I., Thamrin, M., Kamah, M.: Permeability Control on Tompaso Geothermal Field and Its Relationship to Regional Tectonic Setting. Proceedings World Geothermal Congress 2015. Melbourne, Australia, 19-25 April, (2015).

Siahaan, E.E., Soemarinda, S., Fauzi, A., Silitonga, T., Azimudin, T., Raharjo, I.B.: Tectonism and Volcanism Study in the Minahasa Compartment of the North Arm of Sulawesi Related to Lahendong Geothermal Field, Indonesia, Proceedings, World Geothermal Congress 2005 Antalya, Turkey, (2005).

Sumantoro, Z.Z., Yeh, A., O'Sullivan, J., O'Sullivan, M.: Reservoir modelling of Lahendong geothermal field, Sulawesi – Indonesia, Proceedings, 37th New Zealand Geothermal Workshop Taupo, New Zealand (2015).

Sumintadireja, P., Sudarman, S., Zaini, I.: Lahendong geothermal field boundary based on geological and geophysical data. Proceedings, 5th inaga annual scientific conference & exhibitions, Yogyakarta, (2001).

Surachman S.A., Tandirerung T., Buntaran. T.: Assessment of the Lahendong geothermal field, North Sulawesi, Indonesia Proceedings Indonesian Petroleum Association, Sixteenth Annual Convention, (1987)

Utami, P., Widarto, D.S., Atmojo, J.P., Kamah, Y., Browne, P.R.L., Warmada, I. W.: Hydrothermal Alteration and Evolution of the Lahendong Geothermal System, North Sulawesi. Proceedings World Geothermal Congress 2015 Melbourne, Australia, (2015).

Utami, P.: Hydrothermal Alteration and the Evolution of the Lahendong Geothermal System, North Sulawesi, Indonesia. Ph.D. Thesis. The University of Auckland, (2011).

Widagda L. and Jagranatha I.B.: Recharge Calculation of Lahendong Geothermal Field in North Sulawesi-Indonesia, Proceedings, World Geothermal Congress 2005 Antalya, Turkey, (2005).

Yani, A.: Numerical modelling of Lahendong geothermal system, Indonesia geothermal training programme Reports Orkustofnun, Grensásvegur 9, Number 24 IS-108 Reykjavík, Iceland (2006).

Yeh, A., Croucher, A. E., & O'Sullivan, M. J.: Recent developments in the AUTOUGH2 simulator. Proc. TOUGH Symposium 2012. Lawrence Berkeley National Laboratory Berkeley, California, USA. (2012).